AIAA JOURNAL
Vol. 49, No. 3, March 2011

Analysis of Interference Drag for Strut–Strut Interaction in Transonic Flow

Ravi K. Duggirala,* Christopher J. Roy,† and Joseph A. Schetz‡
Virginia Polytechnic Institute and State University, Blacksburg, Virginia 24061

DOI: 10.2514/1.45703

Computational fluid dynamics simulations were performed to predict the interference drag produced by two streamlined struts intersecting at various angles in transonic flow because no relevant experimental data are available for use in design studies. The one-equation Spalart–Allmaras turbulence model was employed in a Reynolds-averaged Navier–Stokes formulation assuming fully turbulent flow. Selected cases were run using the two-equation k-ω shear stress transport turbulence model for comparison. NACA 64A series airfoils with thickness ratios of 5 and 7.5% were studied at Mach 0.8 and 0.85 for intersection angles between 45 and 90 deg at an altitude of 12.2 km (chord-based Reynolds numbers of approximately 5 million). The commercial computational fluid dynamics code FLUENT was used for the analysis. To better understand the flow behavior, contours of surface pressure and velocity near the interaction region were examined. It is observed that the flowfield is disturbed due to shock-induced separation only near the interaction region. There is little effect on viscous drag due to the strut–strut interaction, but changes in the pressure drag result in net interference drag. It is noted that there is an unexpected rise in the interference drag when the struts intersects at 90 deg due to significant shock-induced flow separation on both sides of the intersecting strut, whereas smaller intersection angles show flow separation only on the side with the acute angle. A response surface for the interference drag coefficient as a function of Mach number, thickness ratio, and intersection angle was generated using the numerical simulations for use in the Multidisciplinary Design Optimization studies where efficient means of estimating the interference drag are needed.

Nomenclature

c	=	strut chord, m
L	=	length of a single strut, m
l_c	=	total length for the strut–strut problem, m
M	=	Mach number
M_∞	=	freestream Mach number
P_∞	=	freestream pressure, pa
t	=	strut thickness, m
X	=	streamwise coordinate
Y	=	vertical coordinate
Z	=	transverse coordinate
θ	=	strut–strut intersection angle, deg
ε	=	uncertainty

I. Introduction

SEPARATED flow regions and unwanted shock waves can be produced by the interference between aircraft components in transonic flow. If proper analysis is not done while designing the vehicle, the drag increase associated with such interference will affect the total vehicle performance. Most of the available information for interference drag from struts is limited to low speeds and thick struts [1]. The design of a strut-braced wing for a transonic transport aircraft at a cruise Mach number of 0.85 was previously studied at Virginia Tech using Multidisciplinary Design Optimization (MDO) [2,3]. It was found that the total drag and takeoff gross weight was reduced significantly compared with a conventional cantilever wing arrangement. However, it is critical to analyze and evaluate the interference drag at various junctions such as wing-fuselage and wing-strut junctions. Tétrault et al. [4] conducted a numerical study to predict the interference drag for different angles at which a strut with different thickness ratios intersects a flat surface at different Reynolds numbers. They generated a response surface approximation, and it was observed that the interference drag increases as the angle of the strut deviates from a position perpendicular to the wall. They also observed separated flow at low intersection angles. Based on their study, an engineering rule was proposed that "*If the intersection angle is less than 45 degrees, add a vertical offset*."

The objective of the current study is to predict the interference drag using computational fluid dynamics (CFD) at a strut–strut junction which will be useful while designing strut-braced wings with an offset and also while designing truss-braced wings as shown in Fig. 1. The truss topology introduces several opportunities for improved efficiency. A higher aspect ratio and decreased wing thickness can be achieved without an increase in wing weight relative to a cantilever wing. In addition, the reduction in thickness allows the wing sweep to be reduced without incurring a transonic wave drag penalty. All of these effects enhance opportunities for laminar flow control. However, interference drag from multiple truss member intersections must be carefully analyzed.

II. Problem Description

The objective of this study is to predict the interference drag when two streamlined struts intersect each other at different angles to simulate the truss members found on a strut-braced wing (SBW) and truss-braced wing (TBW). NACA 64A series airfoils with thickness ratios of 5 and 7.5% are studied at Mach 0.8 and 0.85 for intersection angles of 45 to 90 deg at an altitude of 12,192 m ($p_\infty = 19,200$ Pa). For the 1 m chord examined here, these conditions yield Reynolds numbers of 4.7×10^6 and 5×10^6 for Mach 0.8 and 0.85, respectively. These are the typical dimensions of the strut encountered in the course of previous MDO studies [1,3] conducted on the SBW concept. CFD simulations are performed to predict the interference drag with the one-equation Spalart–Allmaras (SA)

Presented as Paper 2009-51 at the 47th AIAA Aerospace Sciences Meeting including The New Horizons Forum and Aerospace Exposition, Orlando, FL, 5–8 January 2009; received 28 May 2009; revision received 24 March 2010; accepted for publication 4 June 2010. This material is declared a work of the U.S. Government and is not subject to copyright protection in the United States. Copies of this paper may be made for personal or internal use, on condition that the copier pay the $10.00 per-copy fee to the Copyright Clearance Center, Inc., 222 Rosewood Drive, Danvers, MA 01923; include the code 0001-1452/11 and $10.00 in correspondence with the CCC.

*Postdoctoral Associate, Department of Aerospace and Ocean Engineering. Member AIAA.
†Associate Professor, Department of Aerospace and Ocean Engineering. Associate Fellow AIAA.
‡Holder of the Fred D. Durham Chair, Department of Aerospace and Ocean Engineering. Lifetime Fellow AIAA.

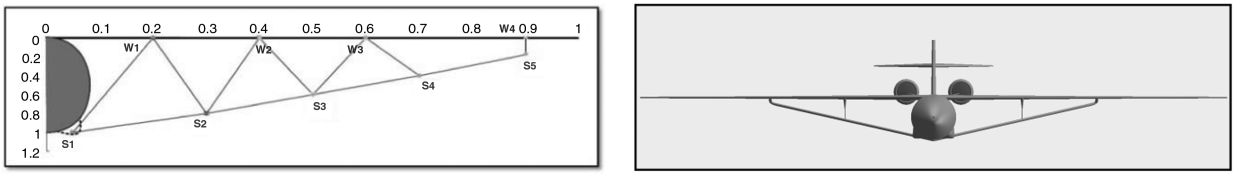

a) b)

Fig. 1 Schematics of a) a multiple-element truss, and (b) MDO design for a simple truss.

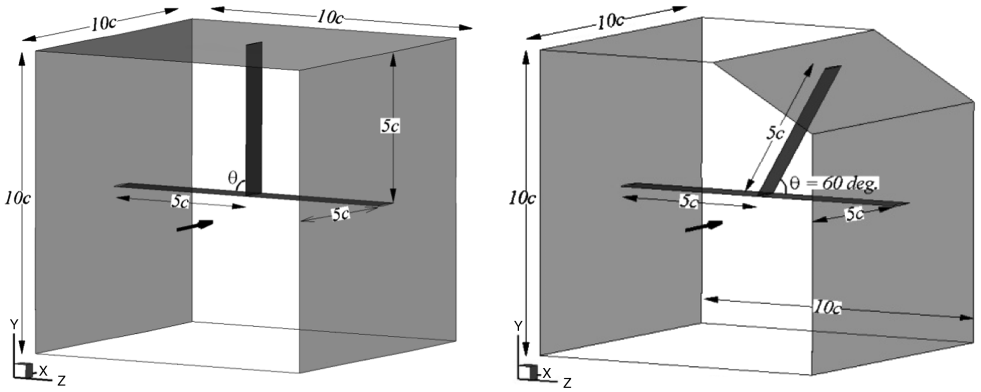

a) b)

Fig. 2 Computational domain for two struts intersecting at a) 90 deg, and b) 60 deg.

turbulence model [5] assuming fully turbulent flow, and a few selected cases were run using the two-equation k-ω shear stress transport (SST) turbulence model [6,7]. FLUENT, [8] a commercial CFD code, is used for the analysis. In the absence of experimental data for the strut-strut configuration, data [9] from a NACA 64A series airfoil with 6% thickness at different angles of attack (0, 2, and 4 deg) were used to perform a validation assessment of the computational model.

Figure 2 gives the details of the computational domain used in this study for 60 and 90 deg intersecting struts. The domain extends five strut chords upstream, downstream, above, and below the strut–strut interaction region to the far-field boundary. The surfaces to the left, right, and top of the interaction region were treated as slip walls. A similar geometric configuration was used for other intersecting angles (45 and 75 deg). Five strut chords was assumed far enough from the junctions to be free of the realized junction effects and this was confirmed by the results below. The goal is to have a computational domain that completely encloses the interaction region and extends far enough that the flow at the boundaries has become 2-D.

III. Numerical Simulation Approach

A. Flow Solver

The Reynolds–averaged Navier–Stokes (RANS) equations were solved for 2-D and 3-D problems with FLUENT, [8] a commercial CFD code. An implicit, upwind, second-order accurate density based solver [8] is used. The turbulence model of Spalart and Allmaras [5], which is commonly used for transonic aerodynamic applications, and selected cases with the two-equation Menter k-ω SST (models [6,7] are employed by integrating to the wall (i.e., without using wall functions). Fully turbulent flow is assumed with early transition assumed to be triggered in the intersection region. First, the problem was solved using a first-order discretization scheme with a CFL number of 1.0 to converge the steady-state iterative residuals by 3 orders of magnitude. Once the residuals were converged to the desired tolerance, a second-order discretization scheme with a CFL number of 10 was used. After performing an iterative error analysis, the final normalized steady-state residual tolerance criteria used in this study is a 5 order of magnitude reduction (10^{-5}), corresponding to an iterative error in the interference drag coefficient of approximately 0.01%.

B. Airfoil Surface Generation

The raw database for the NACA 64A series airfoil sections was obtained from the airfoil generation code LADSON, [10] which produces a blunt trailing edge. To minimize the computational efforts, the upper and lower airfoil surfaces were linearly extrapolated until they intersect, then the final airfoil cross-section is obtained by rescaling in the X-direction to maintain the chord length of 1 m. By scaling in X direction, the t/c at 40% chord has changed by 0.04% (from 0.024991 to 0.024979) for the 5% thick NACA 64A airfoil). The coordinates produced by LADSON code have a poor resolution of 80 data points on the airfoil's upper and lower surface. A third-order spline fit was used to post-process the LADSON coordinates to provide a database with more resolution. The trailing edge obtained from LADSON code and the modified trailing edge for 5% thick NACA 64A airfoil is shown in Fig. 3.

C. Grid Generation

Gridgen [11], a commercial grid generation tool, was used to generate the flowfield mesh. The mesh for 3-D flow solutions has both structured (hexahedral) and unstructured (pyramidal and tetrahedral) cells. The structured grid is used to capture the gradients and resolve the boundary layer near the surface of the airfoil and in the interaction region. The rest of the domain has a mixture of structured and unstructured grid blocks. For 2-D flow solutions, a plane was extracted from the mesh created for the 3-D flow solutions. To perform a grid convergence study, three grid levels (coarse, medium, and fine) were generated. Initially, a fine grid was generated

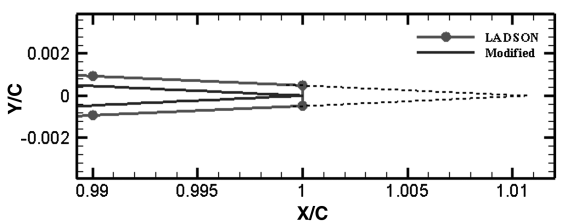

Fig. 3 Trailing-edge closure for 5% thick NACA 64A series airfoil.

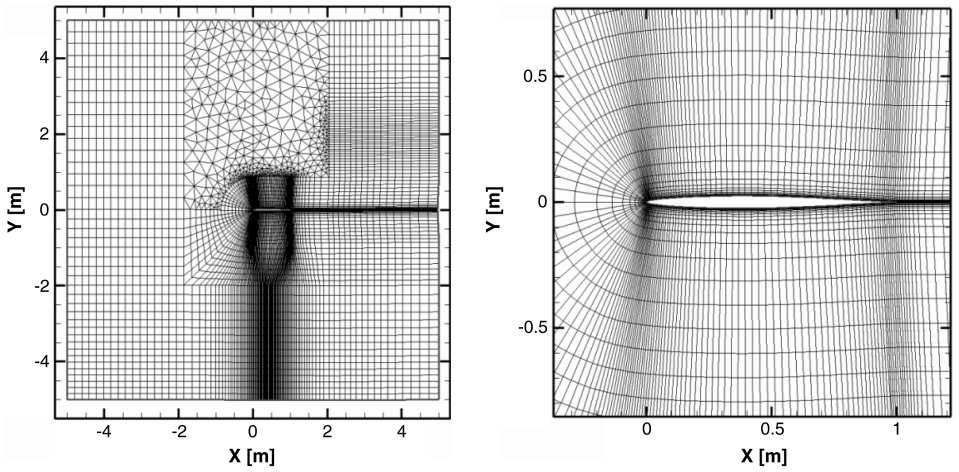

a) b)

Fig. 4 Flowfield mesh (coarse) for 2-D flow simulation: a) hybrid grid in the 2-D computational domain, and b) details of the grid in the vicinity of the airfoil.

and the structured part of the medium grid was obtained from interpolating the grid by removing five grid points and placing three grid points resulting in a coarsening factor of 1.5. The structured part of the coarse grid was obtained by removing every alternate grid point from the fine grid. The unstructured part of medium and coarse grids were automatically generated by the grid generation tool ensuring the local refinement based on the cell volume and the global refinement based on the cell count are nearly equal to the refinement factor of the structured part. The typical grid sizes (medium) used for 2-D and 3-D simulations in this study had approximately 3×10^4 and 5.5×10^6 cells, respectively. Typical flowfield meshes used for 2-D and 3-D simulations are shown in Figs. 4 and 5, respectively.

Figure 4a shows the computational domain used for the flow over a 2-D airfoil where the flow is in the positive X direction. The domain extends five strut chords upstream, downstream, above, and below to the far-field boundary. Since we are integrating to the wall without using wall functions, the first grid point is located at 0.006 mm which results in a maximum y^+ is nearly 1.0 on the coarsest grid. A refined grid around the surface of the airfoil as shown in Fig. 4b is used to resolve the turbulent boundary layer.

Figure 5 shows the flowfield mesh used to study the flow over the strut–strut interaction region. Figure 5a shows the surface mesh on different surfaces (airfoil, slip wall, and far-field boundaries). Figures 5b–5d shows the mesh in constant X, Y, and Z planes,

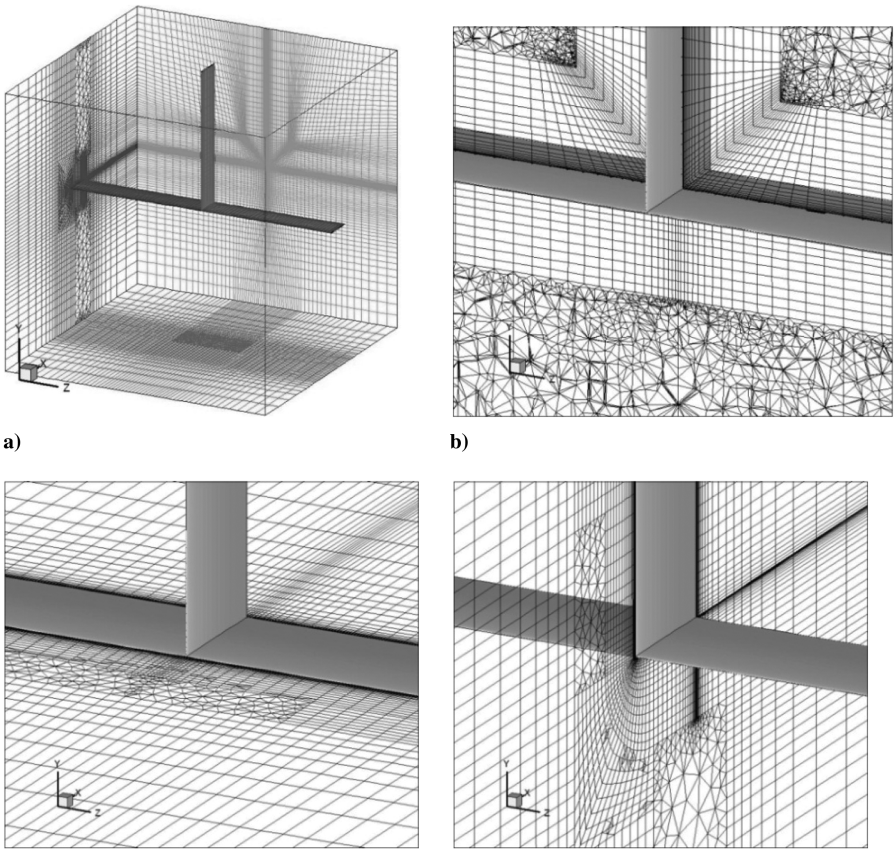

a) b)

c) d)

Fig. 5 Flow field mesh for 3-D flow simulations: a) mesh on the surfaces, b) details of the mesh in a constant X plane, c) details of the mesh in a constant Y plane, and d) details of the mesh in a constant Z plane.

respectively. Figure 5b shows the location where an unstructured grid is used as well as the structured mesh around the airfoil surface with the first grid point located at 0.006 mm which gives a maximum y^+ of 1.0 on the coarsest grid (shown) for these 3D cases.

D. Validation Study

In the absence of experimental data for the 3-D strut–strut interaction, a validation assessment of the computational model was performed on a strut perpendicular to the walls of a wind tunnel performed by Bartelheimer et al. [12], (3-D validation) and also examined a 2-D 64A series airfoil section at various angles of attack under transonic flow conditions (2-D validation). The 2-D validation assessment includes the comparison of pressure coefficient and drag coefficient for a six-inch-long, 6% thick NACA 64A airfoil at angles of attack between 0 and 4 deg and at Mach 0.87. The Mach and the Reynolds numbers reported in experiments were used [9], whereas the static temperature was assumed to be ambient at 300 K. The

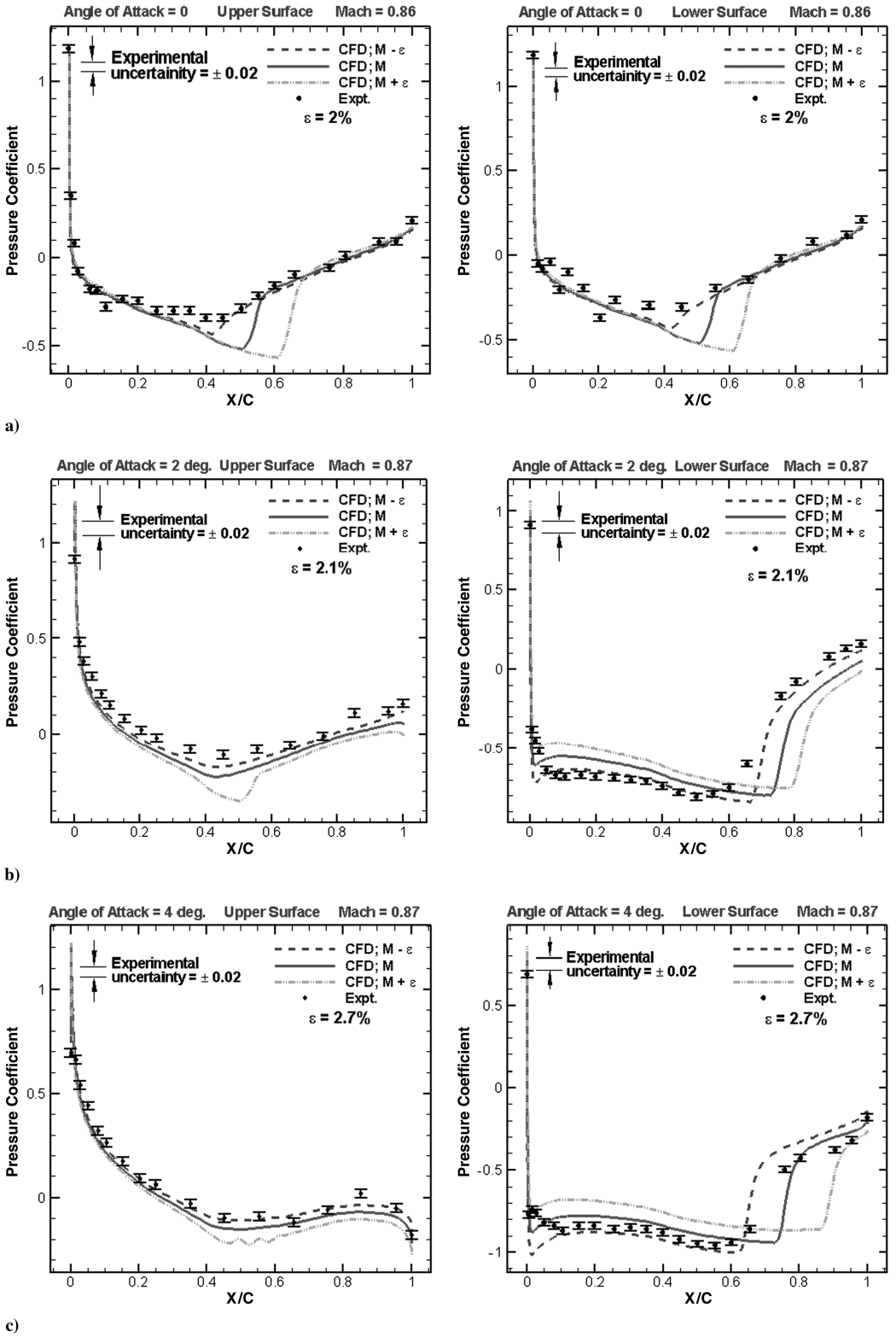

Fig. 6 Validation of pressure coefficient from CFD predictions using experiments [9]; a) AOA = 0 atMach = 0.86, (b) AOA = 2 at Mach = 0.87, and c) AOA = 4 at Mach = 0.87.

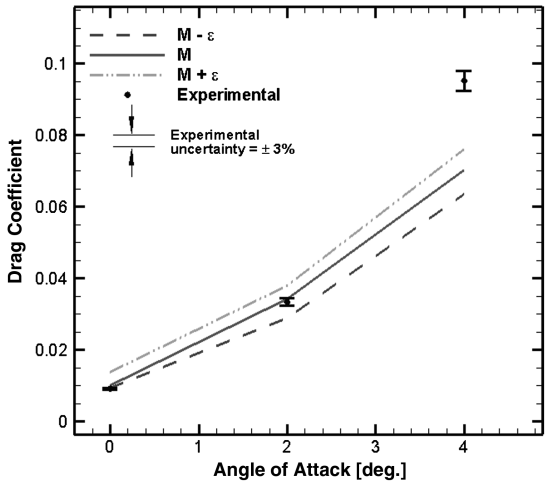

Fig. 7 Validation of drag coefficient from CFD predictions using experiments [9].

Table 1 Boundary-layer properties on the side wind-tunnel wall

	Freestream Mach, M_∞	Reynolds number, Re_c	Displacement thickness δ^*, mm	Momentum thickness θ, mm
Simulation	0.73	6×10^6	2.9626	2.2852
	0.73	5.86×10^6	3.17	2.25
	0.729	5.83×10^6	3.21	2.50
Experiment	0.729	6.09×10^6	3.19	2.48

experiment did not report a location for turbulence transition, so the flow was assumed as fully turbulent and the one-equation SA turbulence model was used.

The computational domain extends 10 chords upstream, downstream, above, and below the airfoil. A grid convergence study was performed using three grid levels for the zero angle of attack case with Mach = 0.87. The estimated error in drag using a grid convergence index (GCI) [13] with a factor of safety of 3.0 is 0.06%, and the observed order of accuracy is 3.5, where the formal order of accuracy is 2. The factor of safety of 3.0 was employed, because the observed order of accuracy did not match the formal order, although the drag did converge monotonically with mesh refinement.

The comparison of pressure coefficient obtained from CFD simulations with experiments for different angles of attack is shown in Fig. 6. The uncertainty for Mach number in the experiments is 2–3%, thus the CFD runs were performed for three Mach numbers: M and $M \pm$ uncertainty. It is observed from Fig. 6 that the pressure coefficient obtained from the simulations at the lower Mach number (M-uncertainty) is in good agreement with the experimental measurements at all three angles of attack. The drag coefficient for the different angles of attack is calculated for three Mach numbers (M, $M \pm$ uncertainty), and the results are compared with experimental measurements in Fig. 7. It is observed that the drag coefficient predicted from the CFD simulations is in good agreement with experimental data for all but the highest angle of attack where the uncertainty in the experimental data is largest.

The 3-D validation assessment includes the comparison of boundary-layer properties along the wind-tunnel wall, pressure coefficient and normal force coefficient along the span of the strut. The experimental data is suitable only for "in-tunnel" CFD validation because the strut was enclosed by solid wind-tunnel walls above, below, and on the sides. The data was not corrected for the effect of blockage. The strut has a span of 340 mm and a chord of 200 mm. The top and bottom walls of wind tunnel are located symmetrically at a distance of 300 mm from the model.

For numerical calculations, strut was modeled with a span of 170 mm only and a symmetry boundary condition was applied to one of the side walls. The inflow and outlet planes were located 3000 mm upstream and 2000 mm downstream of the model, respectively. The Mach and the Reynolds numbers reported in experiments were used [12], whereas the stagnation temperature was assumed to be ambient at 250 K. The location for turbulence transition is reported in

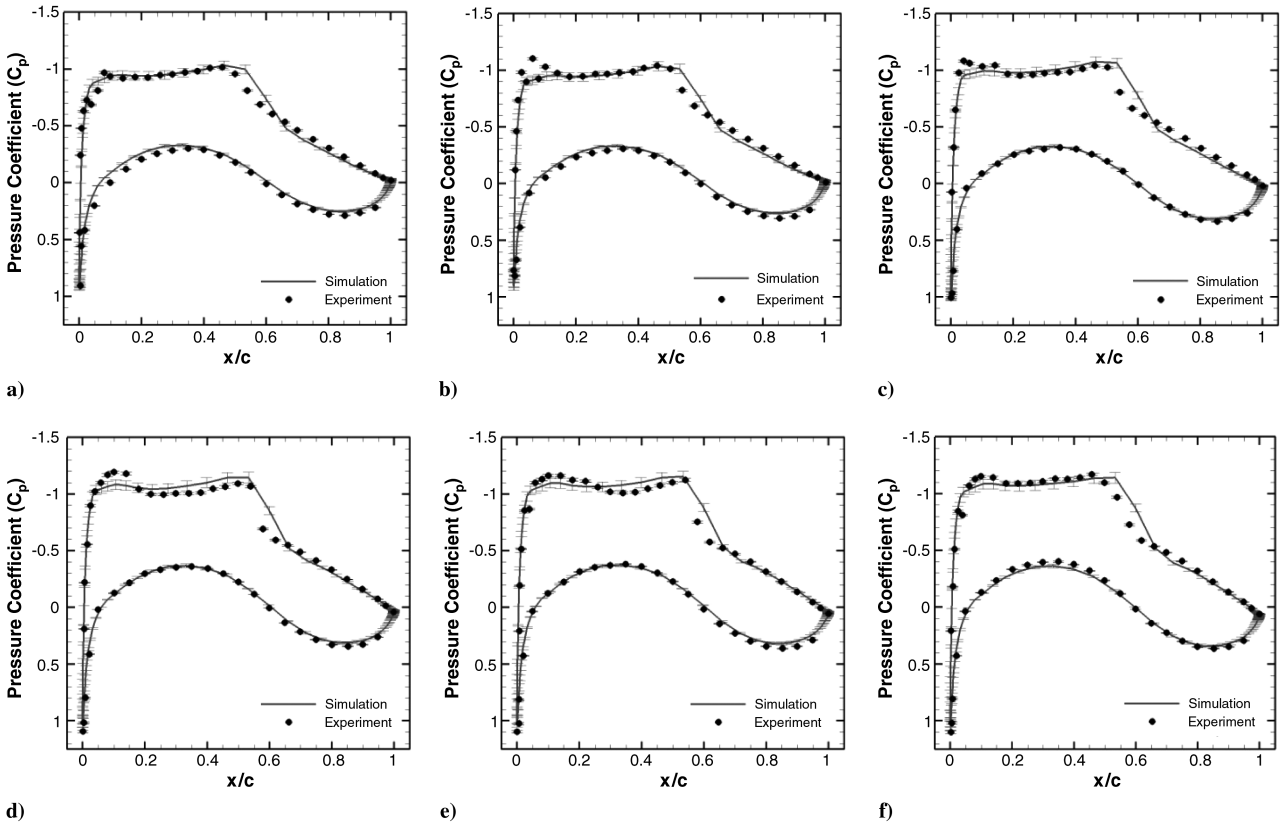

Fig. 8 Pressure coefficient distribution for the validation study, $M_\infty = 0.73$, $\alpha = 1.5°$, $Re_c = 6 \times 10^6$.

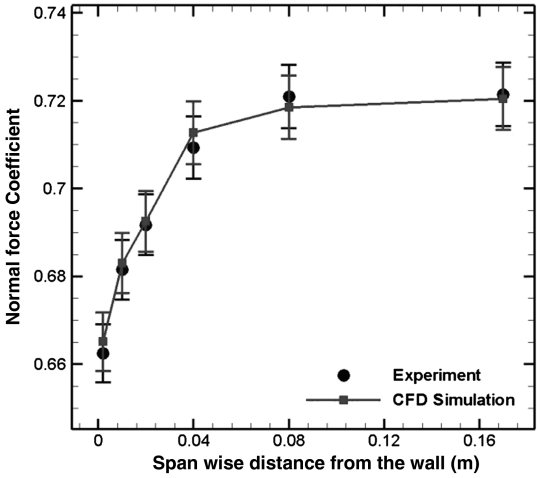

Fig. 9 Normal force coefficient along the wing span for validation study.

experiments was taken to be 6% chord from the leading edge and the one-equation Spalart–Allmaras turbulence model was used.

The freestream Mach number is 0.73, and the Reynolds number is $Re_c = 6 \times 10^6$. The strut makes an angle of 1.50 with respect to the incoming freestream velocity. The side wall boundary-layer properties (displacement thickness and momentum thickness) were compared with the experimental values at 1050 mm upstream of the strut leading edge and reported in Table 1. The predicted values of δ^* and θ are within 8% of the experimental measurements.

The distributions of pressure coefficient along the span of the strut are compared with experimental measuremants and are shown in Fig. 8. The uncertainty in predicting pressure coefficient using simulations (4%), obtained from GCI using factor of safety of 3, and in experimental measurements (1%) were also shown in Fig. 8. The pressure distribution at $\eta = 0.6\%$ is located within the side wall boundary layer. It is observed that the CFD predictions of pressure coefficient are in good agreement with experimental.

The normal force coefficient C_n is computed at each span along the wing, by integrating the pressure coefficient, and is compared against the experimental data in Fig. 9. The CFD simulations overestimated the experimental value of the normal coefficient in the interaction region and underestimated at the middle of the span. However, with the uncertainties in experiments and simulation taken into account, the agreement is generally good and the trend that is seen in experiments (the normal force coefficient increases with the distance from the side wall) is captured by the CFD simulation. With these quite favorable results, we can be confident in applying these CFD tools to model the flow near the junction.

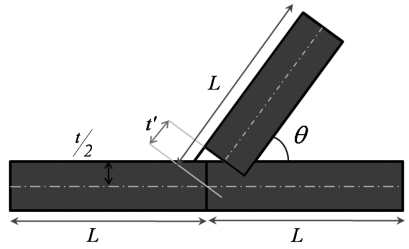

Fig. 10 Strut–strut interaction interference drag calculation approach.

IV. Interference Drag Calculations

The approach adopted to calculate the interference drag using CFD is now discussed. First, 2-D flow over the airfoil is simulated to predict the drag per unit length d'_{2D}. The 3-D "equivalent" drag force without interference is calculated by using the corrected length l_c which is equal to the shaded region in Fig. 10. The total length for the strut–strut problem is taken as $l_c = 3L - t'$ where $t' = \frac{t/2}{\sin\theta}$. The 3-D equivalent drag force without interference is $\bar{\bar{d}}_{3D} = d'_{2D} \times l_c$. The three-dimensional RANS equations were solved to predict the drag d_{3D} for different angles of the strut-strut interaction problem. The difference between the three-dimensional drag with interference and 3-D equivalent drag force without interference gives the net interference drag as defined here

$$d_{\text{int}} = d_{3D} - \bar{\bar{d}}_{3D} \tag{1}$$

The chord c is used to provide the reference area as c^2. The interference drag divided by the dynamic pressure and reference area gives the desired interference drag coefficient

$$c_{d_{\text{int}}} = \frac{d_{\text{int}}}{\frac{\gamma}{2} p_\infty M_\infty^2 c^2} \tag{2}$$

V. Results

A. 2-D NACA64A005 Simulations

In this section numerical simulations are discussed for a 2-D NACA 64A series airfoil with thickness to chord ratio of 5% at Mach 0.8 and 0.85 at an altitude of 12,192 m. For simplicity, we refer to this airfoil section as a NACA64A005.

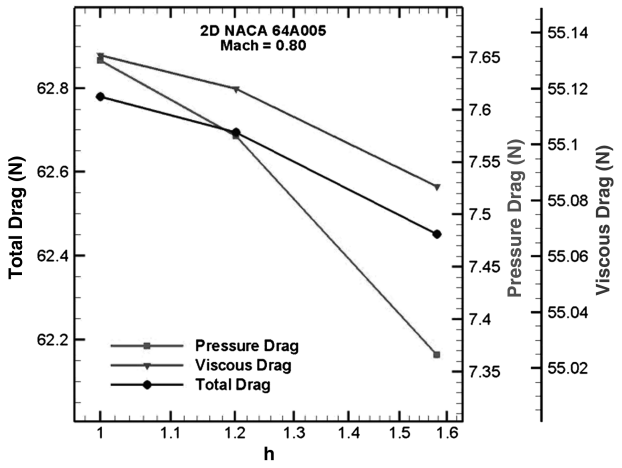

a)

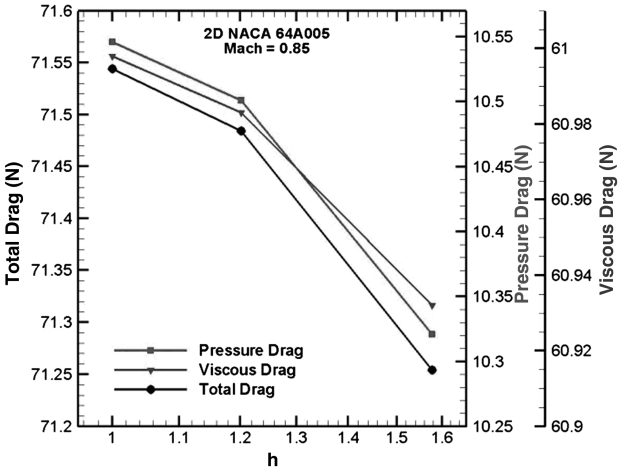

b)

Fig. 11 Grid convergence results for the flow over a 2-D NACA64A005 airfoil.

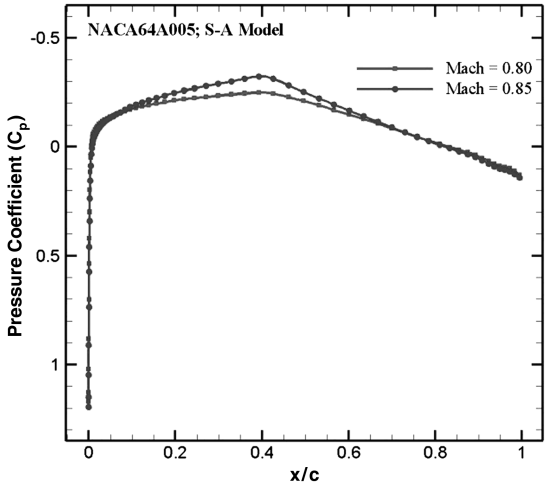

Fig. 12 Coefficient of pressure distribution along the 5% thick airfoil with SA model at Mach = 0.80 and 0.85.

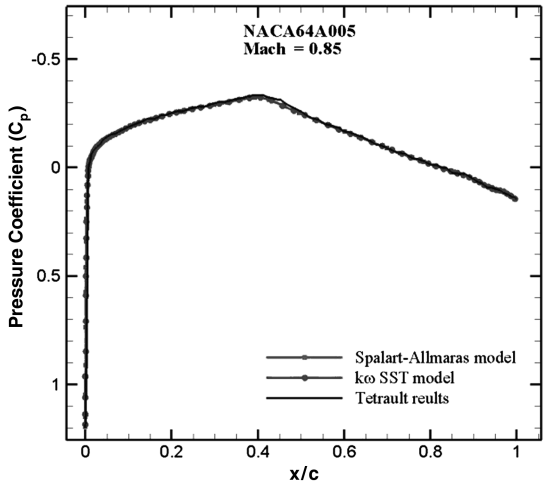

Fig. 13 Coefficient of pressure distribution along the 5% thick airfoil at Mach = 0.85 using SA model, $k\omega$-SST model and previous results from Tétrault [15].

1. Numerical Accuracy:

A grid convergence study was performed for both Mach numbers using three grid levels with the one-equation SA turbulence model. The observed order of accuracy was calculated [14], and the grid convergence index (GCI) [14] was calculated using a factor of safety of 3.0. The details of the grid convergence are shown in Fig. 11. It is observed that the components of drag are changing monotonically with grid refinement. The observed order of accuracy found ranged between 1.85 and 2.8, where the formal order is 2. The estimated errors (from the GCI) in pressure drag, viscous drag, and total drag associated with the medium grid are 3.9%, 0.05%, and 0.52%, respectively, for Mach = 0.80 and 1.7%, 0.1%, and 0.35% for Mach 0.85. Thus, the medium grids were used for the rest of the 2-D simulations with the NACA64A005 airfoil. The iterative error in the total drag prediction on the medium grids is observed to be 0.01% with a normalized iterative residual reduction of 10^{-5}. Thus, a normalized residual tolerance of 10^{-5} was used for the rest of the 2-D NACA64A005 simulations.

2. Numerical Results:

Coefficient of pressure distribution obtained from the numerical simulation using the one-equation SA turbulence model at both Mach numbers are shown in Fig. 12. It is observed that there is no shock formation for this case. Coefficient of pressure distribution for Mach 0.85 from previous work conducted by Tétrault [15] are compared with the coefficient of pressure distribution obtained from simulations using both the one-equation SA and the two-equation, k-ω SST turbulence models in Fig. 13. It is observed that the pressure contours are in good agreement with Tétrault's results.

Pressure, viscous, and total drag obtained from the CFD simulation at Mach 0.85 using both the one-equation SA and the two-equation k-ω SST turbulence models are compared with the previous work by Tétrault [15] in Table 2, which shows that the k-ω SST turbulence model predicted less drag (approximately 5%) compared with SA turbulence model at both Mach numbers. In the previous work by Tétrault [15], an unstructured grid was used in the vicinity of the airfoil whereas in the current research structured grids were used near the airfoil surface which improves the accuracy in capturing the gradients.

B. 2-D NACA64A0075 Simulations

Numerical simulations performed with a 2-D NACA 64A series airfoil with thickness to chord ratio of 7.5% at Mach 0.8 and 0.85 at 12.2 km altitude are discussed. For simplicity, we refer to this airfoil as a NACA64A0075.

1. Numerical Accuracy:

A grid convergence study was performed for both Mach numbers using three grid levels with the one-equation SA turbulence model. The observed order of accuracy was calculated [14] and the grid convergence index [14] was computed with a factor of safety of 3.0. The details of the grid convergence are shown in Fig. 14. The observed order of accuracy ranged between 1.6 and 2, whereas the formal order is 2. Using the GCI, the estimated errors in pressure, viscous, and total drag associated with the medium grid are 0.29, 0.43, and 0.36%, respectively, for Mach = 0.80 and 3, 0.1, and 0.78% for Mach 0.85. Thus, medium grids were used for the rest of the 2-D simulations with the NACA 64A 0075 airfoil. Iterative error in the total drag prediction on the medium grids is seen to be 0.01% with a normalized residual tolerance of 10^{-5}, so the tolerance of 10^{-5} was used for rest of 2-D NACA64A0075 simulations.

2. Numerical Results:

Figure 15 shows the comparison of pressure contours at different Mach numbers, and it is observed that at Mach 0.85 a shock is formed. Coefficient of pressure distribution from the CFD simulations for Mach 0.85 using both the one-equation SA and the two-equation k-ω SST turbulence models were compared with previous work done by Tétrault [15] in Fig. 16. It is observed that the pressure contours from CFD simulation are again in good agreement with the previous work.

Drag (pressure, viscous, and total) predicted from the CFD simulations using both turbulence models (SA and k-ω SST) is tabulated in Table 3 along with the drag predictions from Tétrault [15]. It is observed that in this case also the k-ω SST turbulence

Table 2 Predicted drag using CFD simulations with both turbulence models on medium grids (30 k cells) for NACA64A005

	Mach = 0.8			Mach = 0.85		
	Pressure drag, N/m	Viscous drag, N/m	Total drag, N/m	Pressure drag, N/m	Viscous drag, N/m	Total drag, N/m
Spalart–Allmaras model	7.575	55.120	62.694	10.501	60.983	71.484
$k\omega$ SST model	7.284	52.136	59.420	10.092	57.650	67.743
Tétrault [15]	NA	NA	NA	11.652	58.262	69.914

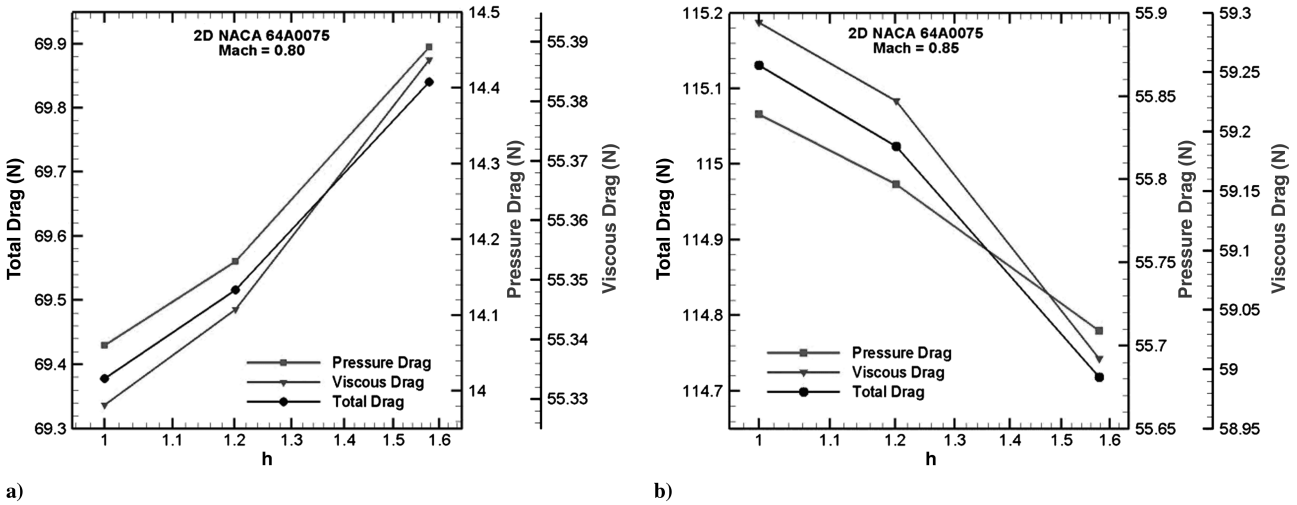

a) b)

Fig. 14 Grid convergence results for flow over 2-D NACA64A0075 airfoil.

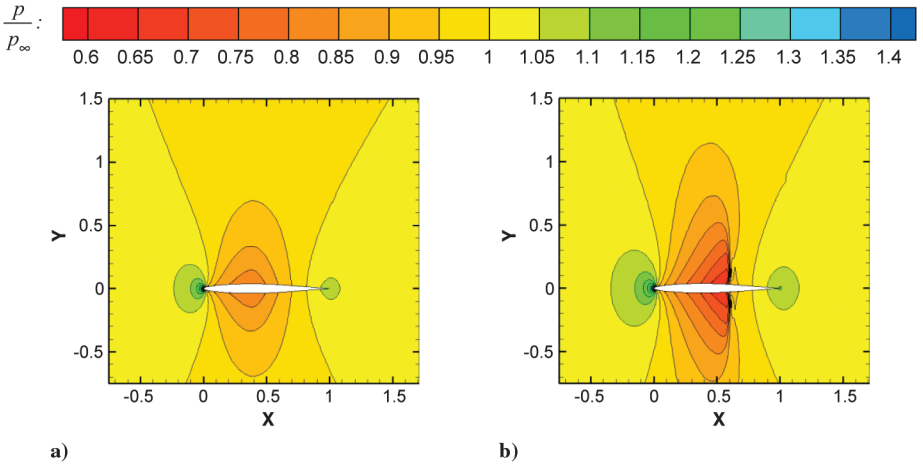

a) b)

Fig. 15 Pressure contours on the medium grid with SA model for 7.5% thickness: a) Mach = 0.80, and b) Mach = 0.85.

model predicted less drag (approximately 4%) compared with SA turbulence model at both Mach numbers. The current work where a structured grid is used in the vicinity of the airfoil predicts a higher total drag with both turbulence models when compared with previous work by Tétrault [15] with an unstructured grid around the airfoil.

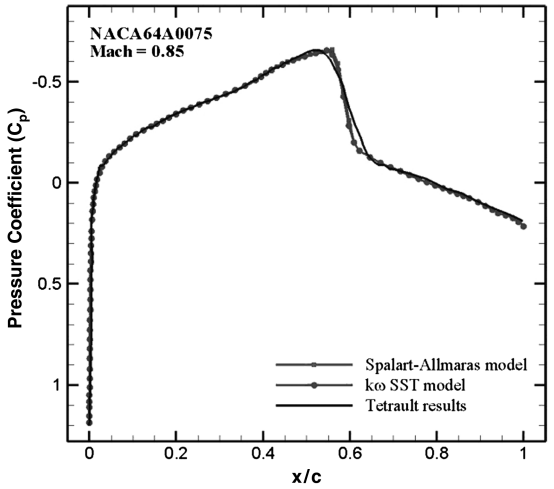

Fig. 16 Coefficient of pressure distribution along the 7.5% thick airfoil at Mach = 0.85 using SA model, $k\omega$-SST model and previous results from Tétrault [15].

C. 3-D NACA64A005 Strut-Strut Interaction Simulations

3-D simulations of NACA64A005 strut-strut intersections at different intersection angles (45, 60, 75, and 90 deg) and Mach numbers (0.80 and 0.85) at an altitude of 12.2 km were performed to calculate the interference drag, and the results are discussed in this section. These results are with SA model.

1. Numerical Accuracy:

A grid convergence study was performed for the 90 deg strut–strut intersection at Mach 0.85 with the one-equation SA turbulence model, and the variation of drag components with grid refinement is shown in Fig. 17. The order of accuracy is 1.7, whereas the formal order is 2. It can be seen that the errors in pressure, viscous, and total drag associated with the medium grid are estimated to be 5, 0.2, and 2%, respectively. Thus, medium grids were used for the rest of the 3-D NACA64A005 strut–strut interaction simulations to estimate the interference drag for different angles of interaction. The iterative error on the medium grids was estimated to be 0.1% with a normalized iterative residual tolerance of 10^{-5} Thus, this residual tolerance was used for the rest of the 3-D NACA64A005 simulations.

2. Numerical Results:

Mach = 0.80:

Distribution of pressure coefficient at 3% chord length above the interaction region on the inside surface (acute angle side) and outside surface (obtuse angle side) are shown in Fig. 18. It is observed that a shock forms for the acute angles of intersection between 40 and 50%

Table 3 Predicted drag using CFD simulations with both turbulence models on medium grids (30 k cells) for NACA64A0075

	Mach = 0.8			Mach = 0.85		
	Pressure drag, N/m	Viscous drag, N/m	Total drag, N/m	Pressure drag, N/m	Viscous drag, N/m	Total drag, N/m
Spalart-Allmaras model	14.171454	55.344551	69.5160050	55.797248	59.225598	115.022846
$k\omega$ SST model	13.17267	52.71411	65.88678	55.13826	56.51084	111.6491
Tetrault [15]	NA	NA	NA	54.378	56.320	110.698

chord. The strength of the shock reduces as the intersection angle increases from 45 to 90 deg. However, for the 90 deg case, weak shocks are formed on both sides of the intersecting struts which can be seen in Fig. 18.

The interference drag and interference drag coefficient were calculated (see Sec. IV), and the results are shown in Table 4 along with the total drag. It is observed that the interference drag decreases with an increase in angle of intersection. As the angle of intersection increases, the strength of the shock decreases, thereby decreasing the amount of shock-induced flow separation which decreases the interference drag.

Table 4 Interference drag details for NACA64A005 at Mach = 0.8 with SA model

	45 deg	60 deg	75 deg	90 deg
Interference drag, N	86.969	67.430	50.391	46.074
Interference drag coefficient	0.0102	0.0079	0.0059	0.0054
Total drag, N	1026.976	1107.46	990.265	985.894

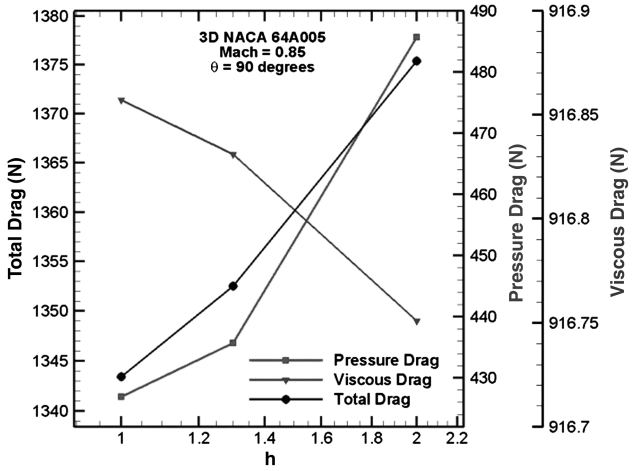

Fig. 17 Grid convergence study for 3-D NACA64A005 strut-strut interaction at Mach = 0.85 and 90 deg.

Mach = 0.85:

The isosurfaces of x-velocity of -1 m/s for all angles of intersections are shown in Fig. 19. The isosurfaces represents the shock-induced flow separation. It is observed that the shock-induced separation is reduced as the intersection angle is increased from 45 to 75 deg. However, when the struts are perpendicular, the flow is symmetric along Y-axis, and shock-induced separation was formed on both sides of the intersection.

The interference drag and interference drag coefficient were calculated and the results with the one-equation turbulence model are shown in Table 5 and are also plotted in Fig. 20. It is observed that the interference drag first decreases as the angle of intersection increases from 45 to 75 deg, then the interference drag increases from 75 to 90 deg. As discussed above, a few cases were run using the two-equation $k\omega$ SST model to see if this unexpected drag rise would be captured by a different turbulence model. It is observed also with the k-ω SST turbulence model that the interference drag increases when the intersection angle increased from 75 to 90 deg which is shown in Fig. 20. This behavior can be explained using Fig. 21 which gives

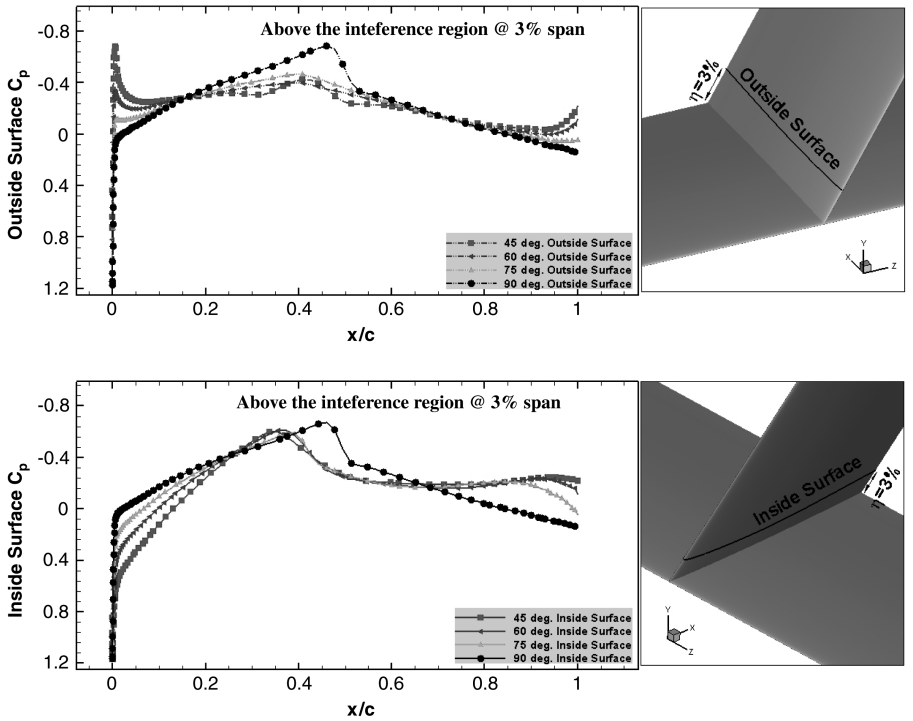

Fig. 18 Distribution of surface pressure coefficient on NACA64A005 strut–strut intersection surface components at Mach = 0.8 with SA model at 3% chord above the intersection.

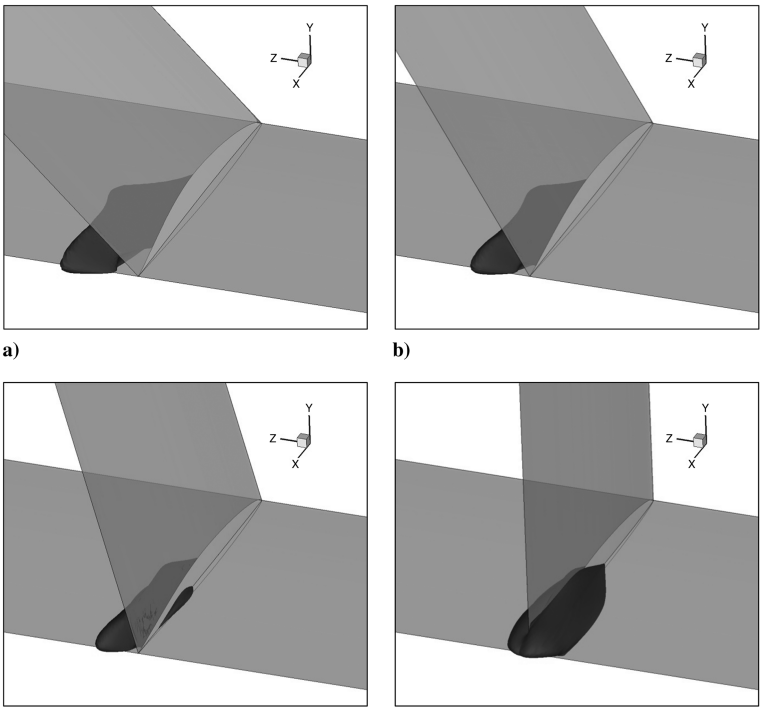

Fig. 19 Flow separation on NACA64A005 strut–strut intersection surface components at Mach = 0.85 with SA model (isosurface of x-veclocity = −1 m/s): a) 45, b) 60 deg, c) 75 deg, and d) 90 deg.

Table 5 Interference drag details for NACA64A005 at Mach = 0.85 using SA model

	45 deg	60 deg	75 deg	90 deg
Interference drag, N	301.277	204.353	159.583	281.225
Interference drag coefficient	0.0310	0.0210	0.0164	0.0290
Total drag, N	1373.083	1275.875	1230.926	1352.507

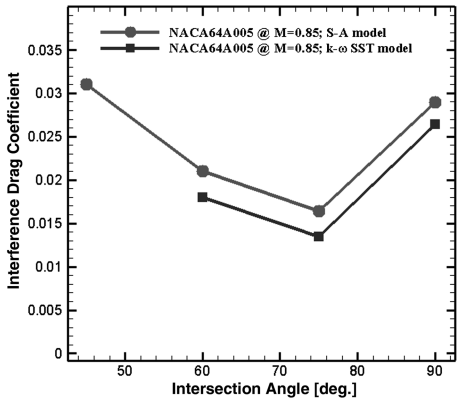

Fig. 20 Effect of intersection angle on interference drag coefficient for NACA64A005 at Mach = 0.85 with different turbulence models.

contours of the axial component of velocity, where reversed flow is indicated by the isosurface. As the angle of intersection increases from 45 to 75 deg, the flow separates only on the acute angle side of the intersection and the separation region decreases. However, for the 90 deg intersection case, the flow separates on both sides of the intersecting strut, thus leading to a significant drag increase.

D. 3-D NACA64A0075 Strut–Strut Interaction Simulations

We now consider 3-D simulations of NACA64A0075 strut–strut interactions at different intersection angles (45, 60, 75, and 90 deg) and different Mach numbers (0.80 and 0.85) at 12.2 km altitude to estimate the interference drag.

1. Numerical Accuracy:

A grid convergence study was performed for the 45 deg strut–strut intersection at Mach 0.80 using the one-equation SA turbulence model, and the drag components at different grid level are shown in Fig. 22. The order of accuracy was found to be 0.9, whereas the formal order is 2. According to Banks et al. [16], the presence of shock reduces the formal order of accuracy to first order. It is noted that the errors in pressure, viscous, and total drag associated with the medium grid are estimated to be 3, 0.2, and 1%, respectively, using the GCI with a factor of safety of 3. Thus, medium grids were used for the rest of the 3-D NACA64A0075 strut–strut interaction simulations to estimate the interference drag for different angles of interaction. Iterative error in the total drag prediction on the medium grids was

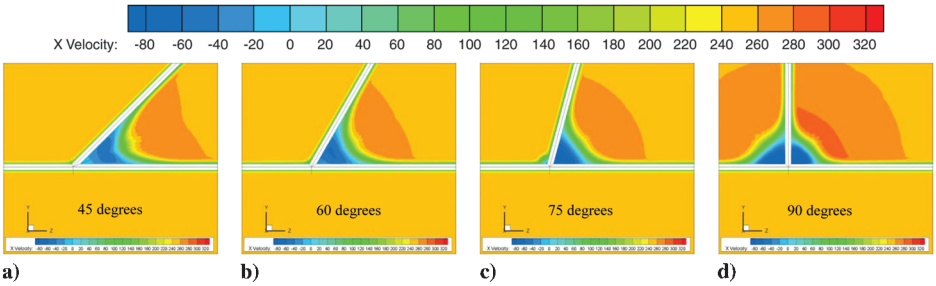

Fig. 21 Axial velocity contours near the interaction region for NACA64A005 at Mach = 0.85 at 80% chord using SA model.

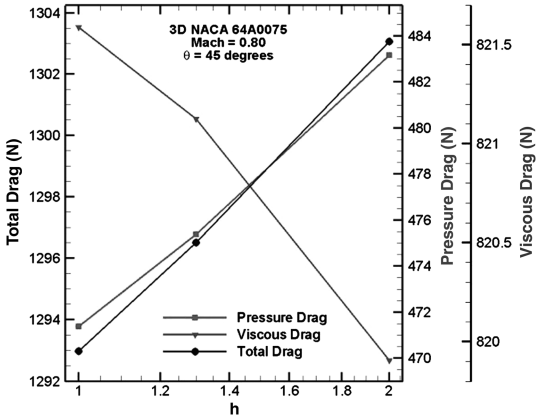

Fig. 22 Grid convergence study for 3*D* NACA64A0075 strut–strut interaction at 45 deg with SA model.

estimated and observed to be 0.1% with a residual tolerance of 10^{-5}, thus this tolerance is used for the rest of 3-D NACA64A0075 simulations.

2. *Numerical Results:*

For simplicity, in this section also the geometry has been divided into six components as shown in Fig. 23e. In this section, contours of the pressure and the velocity will be discussed for NACA64A0075 strut–strut interactions at different angles and different Mach numbers.

Mach = 0.80:

Contours of the pressure on the surfaces of the struts for the NACA64A0075 at Mach 0.8 for different angles of intersection are shown in Fig. 23. It is seen that for all angles of intersection, a stronger shock was formed compared with NACA64A005 cases. The details of the interference drag predicted using the one-equation SA turbulence model are shown in Table 6. The two-equation $k\omega$ SST turbulence model was also used for selected cases (angles of

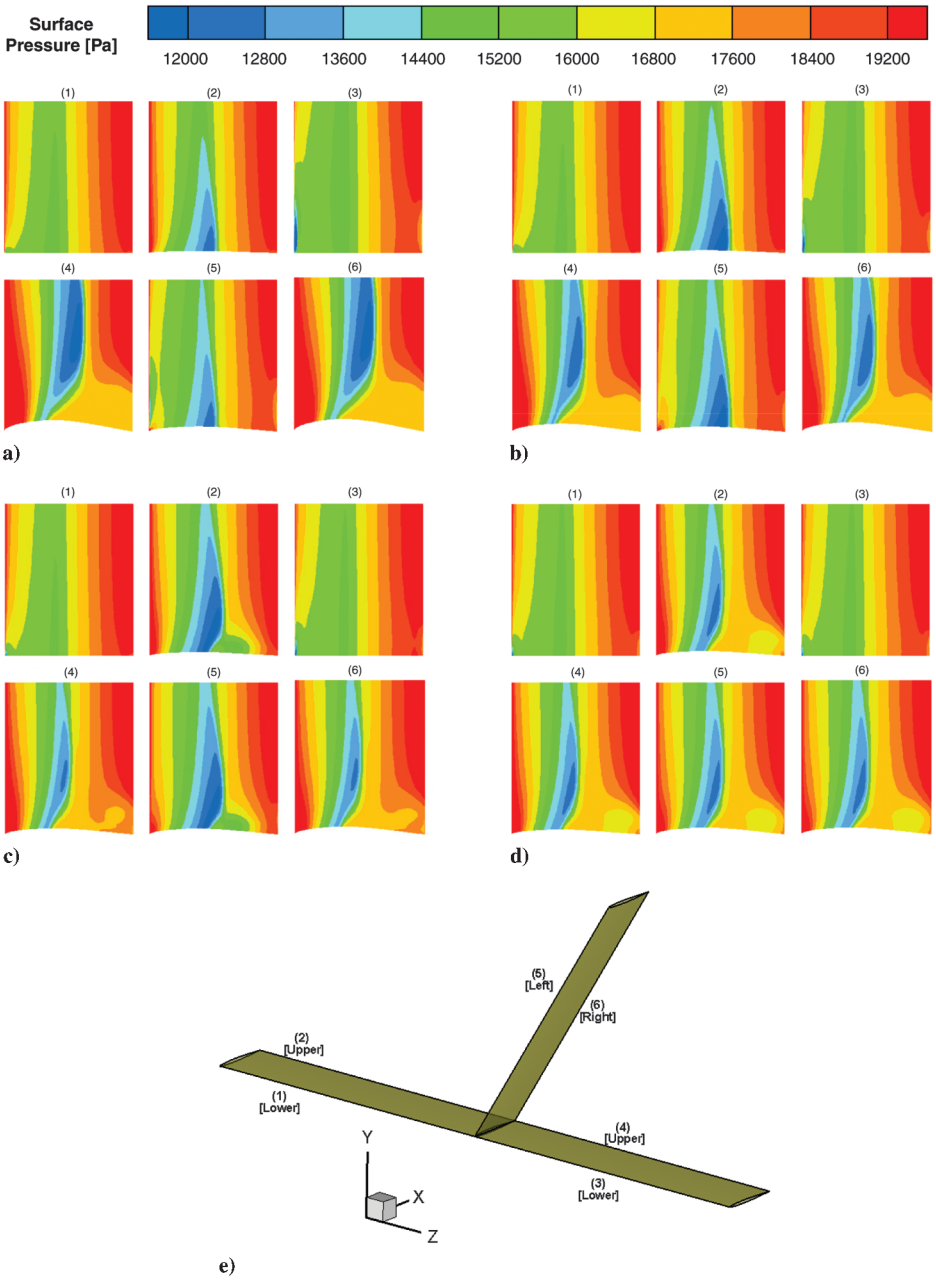

Fig. 23 Surface pressure contours for NACA64A0075 strut-strut intersection surface components at Mach = 0.80 with SA model: a) 45, b) 60, c) 75, and d) 90 deg; e) six surface components of strut–strut geometry.

Table 6 Interference drag details for NACA64A0075 at Mach 0.8 with SA model

	45 deg	60 deg	75 deg	90 deg
Interference drag, N	1099.646	1025.690	1017.256	1041.678
Interference drag coefficient	0.128	0.119	0.118	0.121
Total drag, N	1296.502	1222.545	1214.11	1238.421

intersection of 60, 75, 90) to observe the trend in interference drag with the change in intersection angle. The results obtained from the SA and k-ω SST turbulence models are plotted in Fig. 24. It is observed that the interference drag decreases with an increase in angle of intersection from 45 to 75 deg, whereas when the angle is increased from 75 to 90 deg there is a significant increase in interference drag. This drag increase can be explained using Fig. 25, which shows the axial velocity contours near the interaction region at 80% chord for NACA64A0075 at Mach 0.8.

It is observed from Fig. 25 that the flow separates for all angles of intersection and that the area of separated flow decreases with an increase in the intersection angle from 45 to 75 deg, however, at 90 deg a significant amount of flow separation occurs on both sides of the intersecting strut. Thus, the total area of the separated flow region increases for a 90 deg angle of intersection.

Mach = 0.85:

Predicted surface pressure contours were analyzed with the SA model, and it is observed that a strong shock was formed near 40% chord for all angles of intersection. The details of interference drag calculated using the procedure discussed above are shown in Table 7.

A similar trend of first decreasing drag with an increase in angle from 45 to 75 deg and then increasing drag from 75 to 90 deg is also

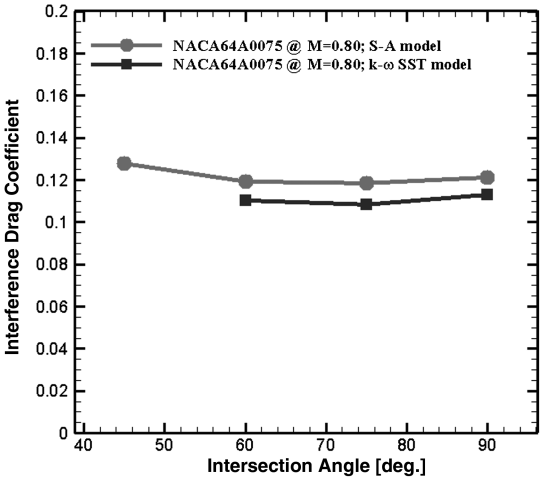

Fig. 24 Effect of intersection angle on interference drag coefficient for NACA64A0075 at Mach = 0.80 with different turbulence models.

Table 7 Interference drag details for NACA64A0075 at Mach = 0.85

	45 deg	60 deg	75 deg	90 deg
Interference drag, N	2127.179	1899.457	1852.317	1866.493
Interference drag coefficient	0.219	0.196	0.190	0.192
Total drag, N	2959.950	2732.228	2685.088	2698.792

observed for this case. Figure 26 shows the axial velocity contours near the interaction region at 80% chord. The figure also shows that the flow separates for all angles of intersection. The area of the separated region first decreases with an increase in angle of intersection from 45 to 75 deg and then the total area of separated flow increases for a 90 deg angle of intersection as the flow separates on both sides of the strut.

E. Interference Drag Response Surface

Numerical simulations for the strut–strut interaction problem were performed by varying the Mach number, the angles of interaction, and the thickness of the airfoil cross section. Based on the results obtained from those simulations, a response surface for the interference drag coefficient as a function of thickness ratio and intersection angle was generated for both Mach numbers as shown in Fig. 27. The response surfaces, or analytical approximations thereof, can be extremely useful in preliminary MDO studies of truss-braced wings where rapid aerodynamic prediction is needed. It is observed that at Mach = 0.85, for both thicknesses, the interference drag increased at 90 deg due to shock-induced flow separation on both sides of the interaction region. Whereas for Mach = 0.8 at the lower thickness, the interference drag decreases monotonically with an increase in angle of interaction. For Mach 0.8 at higher strut thickness, the interference drag again increased at a 90 deg intersection due to shock-induced separation on both sides of the strut.

MATLAB was employed to fit a quadratic response surface to the interference drag coefficient using a standard least-squares procedure. Separate response surface was generated for different Mach numbers. These equations can be included in design studies to account for the interference drag penalty of the junctions. The response surface can be written as:

For Mach number = 0.80:

$$-0.0455 - 0.1836\sin\theta + 1.5424(t/c) + 0.1108\sin^2\theta + 27.4626(t/c)^2 - 0.4234(t/c)\sin\theta \quad (3)$$

For Mach number = 0.85:

$$-0.0037 - 0.6116\sin\theta + 5.4198(t/c) + 0.4299\sin^2\theta + 33.2422(t/c)^2 - 2.8708(t/c)\sin\theta \quad (4)$$

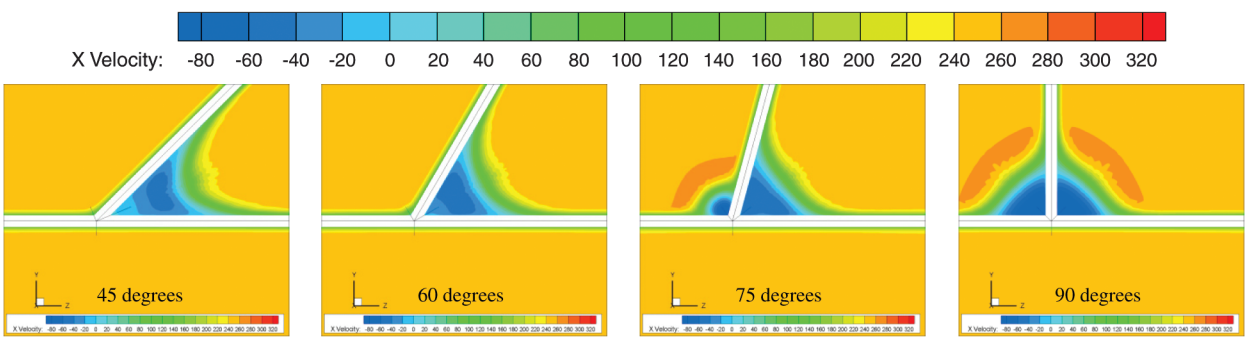

Fig. 25 Axial velocity contours near the interaction region for NACA64A0075 at Mach 0.80 at 80% chord with SA model.

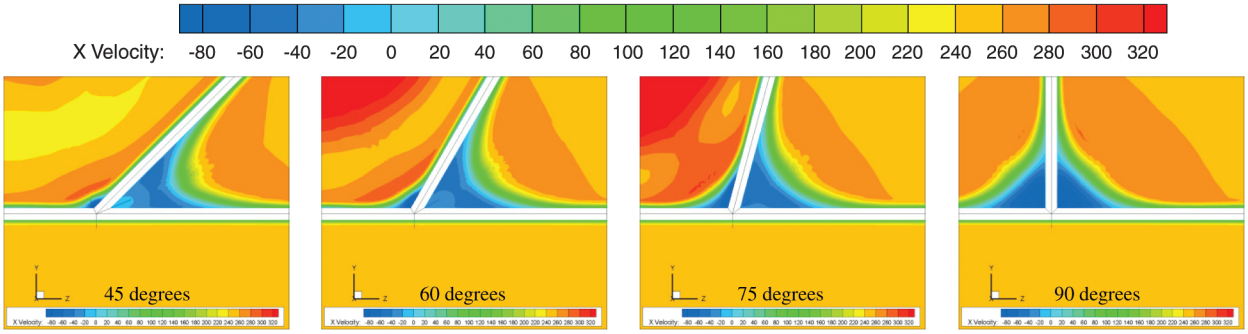

Fig. 26 Axial velocity contours near the interaction region for NACA64A0075 at Mach 0.85 at 80% chord with SA model.

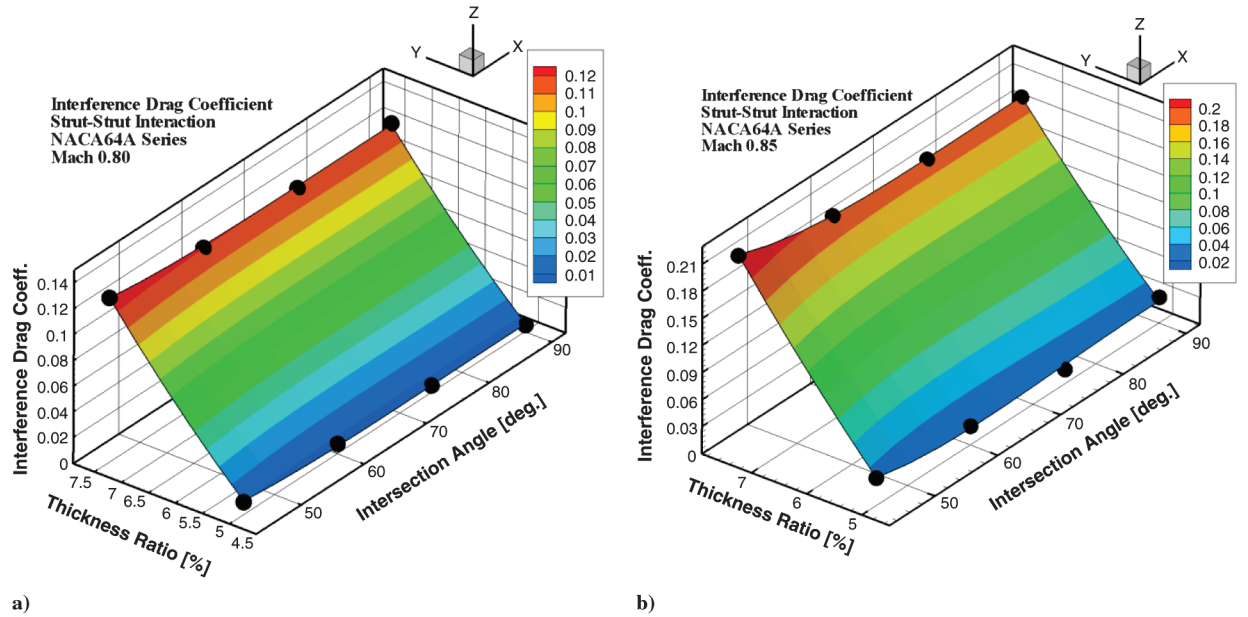

Fig. 27 Response surface with contours of interference drag: a) Mach 0.8 and b) Mach 0.85.

VI. Conclusions

In this study, the RANS equations were solved with the SA turbulence model to simulate the flow past a strut-strut intersection at transonic speeds to determine the interference drag of such junctures. Selected cases were also run using the two-equation, k-ω SST turbulence model to study the trends with different turbulence models. NACA 64A series airfoils with thickness ratios of 5 and 7.5% were studied at Mach 0.8 and 0.85 for intersection angles between 45 and 90 deg at a simulated altitude of 12.2 km. These conditions yielded a Reynolds number based on the strut chord of approximately 5 million, thus fully turbulent flow was assumed. Simulations over 2-D airfoils were found to be in good agreement with previous CFD results [15] as well as experimental data [9]. A detailed grid convergence study was performed for both 2-D and 3-D cases. The GCI was calculated and resulted in grid-related uncertainties of approximately 2% for the NACA64A005 and 1% for NACA64A0075 cases. Contours of surface pressure and axial flow velocities were analyzed, and interference drag coefficients were calculated. A response surface was generated for both Mach numbers with contours of interference drag. In addition to characterizing the interference drag coefficient as a function of Mach number, strut thickness, and intersection angle, the most important finding in this study was the presence of an unexpected drag rise when the struts intersected at 90 degrees relative to the smaller intersection angles. It was observed that at Mach 0.85, for both thicknesses, the interference drag increased at a 90 deg intersection angle compared with the 75 deg intersection angle due to shock-induced flow separation on both sides of the intersecting strut. For Mach 0.8 at the lower thickness, the interference drag decreased monotonically with increase in the angle of intersection. At the higher 7.5% thickness, the interference drag again increased for the 90 deg intersection due to shock-induced separation on both sides of the strut. This drag rise was caused by the presence of significant flow separation on both sides of the strut intersections, whereas at lower intersection angles, the flow tended to separate only on the acute angle side. Also, the magnitude of the interference drag coefficient is larger than that found in prior CFD simulations of a strut intersecting a flat plate [15].

In the future, additional turbulence models, including large eddy simulation (LES) and hybrid RANS-LES, should be examined. Higher thickness ratios as well as different airfoil cross sections should be studied. The current study could be extended by lowering the intersection angles, running at different Mach numbers, and examining different angles of attack (the local angle of attack for a strut–strut intersection is difficult to predict for a full transport aircraft). Also, it would be of interest to study different geometries such as one-sided strut intersections and three-member intersections, which are commonly seen in truss-braced wings as evidenced by Fig. 1. The parameter space of interest is very large, and cases with intersections of truss members with different thickness ratios and for different chords need to be considered. Finally, experimental studies of strut–strut intersections are surely needed to perform rigorous validation assessments of CFD with different turbulence models for a complex flow problem such as the one studied here.

Acknowledgments

This work is sponsored by NASA Langley Research Center through the National Institute for Aerospace under contract VT-03-1, 2649-VT, SUPP87.

References

[1] Hoerner, S. F., "Fluid Dynamic Drag," Hoerner Fluid Dynamics, Brick Town, NJ, 1965.

[2] Gern, F. H., Gundlach, J. F., Ko, A., Naghshineh-pour, A. H., Sulaeman, E., Tétrault, P.-A., Grossman, B., Kapania, R. K., Mason, W. H., Schetz, J. A., and Haftka, R. T., "Multidisciplinary Design Optimization of a Transonic Commercial Transport with a Strut-Braced Wing," *World Aviation Congress*, WAC Paper 1999-01-5621, Oct. 1999.

[3] Gundlach, J. F., Tétrault, P.-A., Gern, F. H., Naghshineh-Pour, A. H., Ko, A., Schetz, J. A., Mason, W. H., Kapania, R. K., Grossman, B., and Haftka, R. T., "Conceptual Design Studies of a Strut-Braced Wing Transonic Transport," *Journal of Aircraft*, Vol. 37, No. 6, 2000, pp. 976–983.
doi:10.2514/2.2724

[4] Tétrault, P.-A., Schetz, J. A., and Grossman, B., "Numerical Prediction of Interference Drag of Strut-Surface Intersection in Transonic Flow," *AIAA Journal*, Vol. 39, No. 5, May 2001, pp. 857–863.
doi:10.2514/2.1389

[5] Spalart, P. R., and Allmaras, S. R., "A One-Equation Turbulence Model for Aerodynamic Flows," AIAA Paper 92-0439, Jan. 1992.

[6] Menter, F. R., "Two-Equation Eddy-Viscosity Turbulence Models for Engineering Applications," *AIAA Journal*, Vol. 32, No. 8, August 1994, pp. 1598–1605.
doi:10.2514/3.12149

[7] Menter, F. R., Kuntz, M., and Langtry, R., "Ten Years of Experience with the SST Turbulence Model," *Turbulence, Heat and Mass Transfer 4*, Begell House Inc., Redding, CT, 2003, pp. 625–632.

[8] Fluent 6.3 User's Guide, Vols. 1–3, 2007.

[9] Stivers, L. S., Jr., "Effects of Subsonic Mach Numbers on the Forces and Pressure Distributions on Four NACA 64A- Series Airfoil Section at Angle of Attack as High as 28°," NACA Technical Note 3162, Sept. 1954.

[10] Ladson, C. L., and Brooks, C. W., Jr., "Development of a Computer Program to Obtain Ordinates for NACA 6- and 6A- Series Airfoils," NASA TM X-3069, Sept. 1974.

[11] Gridgen 15.11 User's Guide, 2007.

[12] Bartelheimer, W., Horstman, K. H., and Puffert-Meissner, W., "2*D* Airfoil Tests Including Side Wall Boundary Layer Measurements," *A Selection of Experimental Test Cases for the Validation of CFD Codes*, AGARD, Advisory Rept. 303, 1994.

[13] Roache, P. J., *Verification and Validation in Computational Science and Engineering*, Hermosa Publishers, Socorro, NM, 1998.

[14] Roy, C. J., "Review of Code and Solution Verification Procedures for Computational Simulation," *Journal of Computational Physics*, Vol. 205, No. 1, 2005, pp. 131–156.
doi:10.1016/j.jcp.2004.10.036

[15] Tétrault, P.-A., "Numerical Prediction of the Interference Drag of a Streamlined Strut Intersecting a Surface in Transonic Flow," Ph.D. Dissertation, Aerospace and Ocean Engineering Department, Virginia Polytechnic Inst. and State Univ., Blacksburg, VA, 2000.

[16] Banks, J. W., Aslam, T., and Rider, W. J., "On Sub-linear Convergence for Linearly Degenerate Waves in Capturing Schemes," *Journal of Computational Physics*, Vol. 227, No. 14, 2008, pp. 6985–7002.
doi:10.1016/j.jcp.2008.04.002

S. Fu
Associate Editor